Journal of Polymers and the Environment (2021) 29:121–129
https://doi.org/10.1007/s10924-020-01856-y

ORIGINAL PAPER

Modification of Poly(Lactic Acid) Rheological Properties Using Ethylene–Vinyl Acetate Copolymer

Daisuke Kugimoto[1] · Shingo Kouda[1] · Masayuki Yamaguchi[2]

Published online: 19 August 2020

Abstract
The effect of ethylene–vinyl acetate copolymer (EVA) addition on the rheological properties of poly(lactic acid) (PLA) was studied. EVA exhibited strain-hardening behavior in the transient elongational viscosity due to its long-chain branch structure, whereas PLA did not show any strain-hardening. The blends showed sea-island structure, in which the size of EVA droplets decreased with the vinyl acetate content in EVA. It should be noted that the blends showed strain-hardening behavior even though EVA is not in the continuous phase. During elongational flow, EVA droplets deform to the fibrous shape owing to hydrodynamic force applied by the matrix PLA, and eventually their deformation is greatly reduced as a result of the strain-hardening. Consequently, the blend system behaved like a rigid-fiber dispersion, which are known to show enhanced elongational viscosity. Finally, the processability of a tubular-blown film was improved by the EVA addition because of the strain-hardening.

Keywords Poly(lactic acid) · Rheological properties · Elongational viscosity · Polymer blends

Introduction

Poly(lactic acid) (PLA)—a biodegradable plastic produced from renewable resources—has several advantages including biodegradability, rigidity, and transparency [1–4]. However, PLA has limited applications owing to its less advantageous properties such as mechanical brittleness, slow crystallization, and low melt elasticity. In particular, poor processability attributed to low melt elasticity is a significant limitation for various processing operations such as T-die extrusion, tubular-blown film extrusion, blow-molding, thermoforming, and foaming, in which marked strain-hardening in the transient elongational viscosity is required [3, 5–11]. This problem is not only encountered for PLA, but also various types of biomass-based polyesters because they have narrow molecular weight distributions and no long-chain branches. Various techniques have therefore been proposed to provide strain-hardening, one of the most important elastic properties in the molten state, to improve the processability.

It is well known that a polymer with long-chain branches shows marked strain-hardening in the transient elongational viscosity. In the case of conventional PLA, a linear polymer is obtained by ring-opening polymerization of lactide. Therefore, introducing a multi-functional monomer into the polymerization process as a branch point to provide long-chain branches has been reported [12, 13]. The incorporation of long-chain branches can also be achieved by the addition of a reactive compound to molten linear PLA. In particular, commercially available ethylene–acrylate copolymers containing glycidyl function are effective for enhancing the melt elasticity of various polyesters including PLA [14–16]. Furthermore, the addition of flexible nanofibers to provide strain-hardening behavior in the transient elongational viscosity has been proposed [17–20], and is currently an available technique in industry.

Recently, mixing with an immiscible polymer with long-chain branches has been proposed as a simple method of achieving strain-hardening. However, to date, only one system—the addition of low-density polyethylene (LDPE) to polypropylene (PP)—has been reported [21–23]. Strain-hardening behavior in the transient elongational viscosity was clearly detected for the blend system, although LDPE

✉ Masayuki Yamaguchi
m_yama@jaist.ac.jp

[1] Polymer Materials Research Laboratory, Tosoh Corporation, 1-8 Kasumi, Yokkaichi, Mie 510-8540, Japan

[2] School of Materials Science, Japan Advanced Institute of Science and Technology, 1-1 Asahidai, Nomi, Ishikawa 923-1292, Japan

was a dispersed phase. During the initial stage of elongational flow, LDPE droplets were deformed into fibrous shapes in a continuous PP phase. Eventually, they were barely deformed owing to their strain-hardening behavior. Consequently, the system behaved like a dispersion of rigid fibers. It is known that the steady-state elongational viscosity of a dispersed-fiber system is greater than three times the zero-shear viscosity due to excess deformation of the continuous phase between neighboring fibers [24–26]. As a result, PP/LDPE blends show strain-hardening in the transient elongational viscosity. Such mechanisms are assumed to be applicable for various polymer blends in which a dispersed phase shows strain-hardening in the elongational viscosity, however, to the best of our knowledge, there have been only one report [27] other than for PP/LDPE.

In this study, ethylene–vinyl acetate copolymer (EVA), which has a long-chain branch structure [28] and thus shows strain-hardening in its elongational viscosity [29], was therefore used to modify the rheological properties of PLA. In addition, the processability of PLA/EVA in tubular-blown film extrusion was evaluated. Since PLA is known to be miscible with poly(vinyl acetate) [30], good compatibility is expected based on the findings of our preceding paper [4].

Experimental

Materials

A commercially available poly(lactic acid) (PLA) (Ingeo 4032D; NatureWorks) with an L-lactide content of 98.5% and a melting point of 167 °C was used. Furthermore, two types of ethylene–vinyl acetate copolymer (EVA) with different vinyl acetate (VAc) contents were used, EVA25 (Ultrathene 640; Tosoh) and EVA80 (Levapren 800; Lanxess). The numerals in the EVA sample codes represent the VAc content as a weight fraction. EVA25 was a crystalline polymer and had a melting point of approximately 75 °C, while EVA80 was amorphous. The details of the sample characteristics were mentioned in our previous paper [4]. The solubility parameters, calculated using the group contribution method proposed by Small [31], were as follows [4]: 19.6 $MPa^{0.5}$ for PLA, 17.7 $MPa^{0.5}$ for EVA25, and 18.6 $MPa^{0.5}$ for EVA80.

Blend Preparation

Both PLA and EVA were dried at 80 °C for 3 h to avoid hydrolysis [32], then mixed in the molten state using an internal batch mixer (Labo-Plastmill; Toyo Seiki Seisaku-Sho, Japan) at 180 °C for 5 min. The blade rotation speed was 120 rpm, which provided a shear rate of 114 s^{-1} between the blades and the inner wall. The blend ratio of PLA/EVA in weight was 80/20. Thermal stabilizers such as pentaerythritol tetrakis(3-(3,5-di-tertbutyl-4-hydroxyphenyl) propionate) (Irganox 1010; Ciba Specialty Chemicals, Switzerland) and 6-[3-(3-tert-butyl-4-hydroxy-5-methylphenyl)propoxy]-2,4,8,10-tetra-tert-butyldibenzo [d,f] [1,3,2] dioxaphosphepin (Sumilizer GP; Sumitomo Chemical, Japan) were added. The content of each stabilizer was 3000 ppm. The blend samples were compression-molded into flat sheets with various thicknesses at 200 °C, then quenched at 25 °C.

Film Processing

The tubular-blown film processability was evaluated using a single-screw extruder (EX-50, Placo, Japan) with an annular die with a diameter of 75 mm and a gap of 1.25 mm. After mixing the polymer pellets at room temperature, they were fed into a hopper feeder with an output rate of 12 kg/h. The temperature at the die was set at 200 °C and the blow-up ratio was 2.5. Two types of film with different thickness, i.e., 10 and 30 μm, were prepared. The take-up speed was 9.0 m/min and the take-up ratio was 16 for the 30 μm-thick film. In the case of the 10 μm-thick film, the take-up speed was 27.0 m/min and the take-up ratio was 48.

Measurements

The frequency dependence of oscillatory shear moduli in the molten state, such as storage modulus G' and loss modulus G'', was measured using a cone-and-plate rheometer (ARES G2; TA instruments, DW) at various temperatures (170, 190, and 210 °C). The angle of the cone was 0.1 rad and its diameter was 25 mm. Steady-state shear properties, such as shear stress and primary normal stress difference, were also measured at 170 °C. The growth curves of the transient uniaxial elongational viscosity were obtained using the same instrument equipped with a universal testing platform at 170 °C. Rectangular samples 10 mm wide, 15 mm long, and 0.6 mm thick were used.

The blend morphology was examined using a scanning electron microscope (SEM; TM3030; Hitachi, Japan). Prior to SEM observation, the cryogenically fractured surface of the compression-molded sheet was coated with gold. The diameters of the dispersed EVA particles were determined from the SEM images using image analysis software (Image J; National Institutes of Health, MD).

The mechanical properties were evaluated at 25 °C using the films with 30 μm thickness obtained using the tubular-blown method. The tensile tests were carried out using a tensile testing machine (Tensilon RTE-1210; Orientec, Japan) at a crosshead speed of 500 mm/min. The samples were cut into dumbbell-shaped specimens (JIS Z 1702). The tear strength was evaluated with an Elmendorf-type tearing tester (Toyo Seiki Seisaku-sho, Japan). Both the tensile

properties and tear strength tests, which were carried out for both machine and transverse directions (MD and TD), were performed five times for each sample.

Results and Discussion

Characteristics of the Pure Polymers

The master curves of the oscillatory shear moduli for pure samples are shown in Fig. 1 as a function of angular frequency ω. The reference temperature T_r was 170 °C. The apparent flow activation energy ΔE_a, calculated from the Arrhenius plot, is denoted in the figure. Both EVA25 and EVA80 showed a broad distribution of relaxation times compared with PLA. This was as expected because EVA has a broad molecular weight distribution with long-chain branch structure [4]. In contrast, PLA showed rheological terminal region clearly; i.e., $G' \propto \omega^2$ and $G'' \propto \omega$ in the low frequency region. The zero-shear viscosities, determined using Eq. (1), at 170 °C for the polymers are as follows; 8.2 kPa s for PLA, 12.4 kPa s for EVA25, and 7.2 kPa s for EVA80.

$$\eta_0 = \lim_{\omega \to 0} \frac{G''}{\omega} \tag{1}$$

Strictly speaking, both EVA samples exhibited thermorheologically complex behavior. Figure 2 shows the van Gurp-Palmen plots [33] for the pure polymers. It was found that the data at higher temperature deviated upward

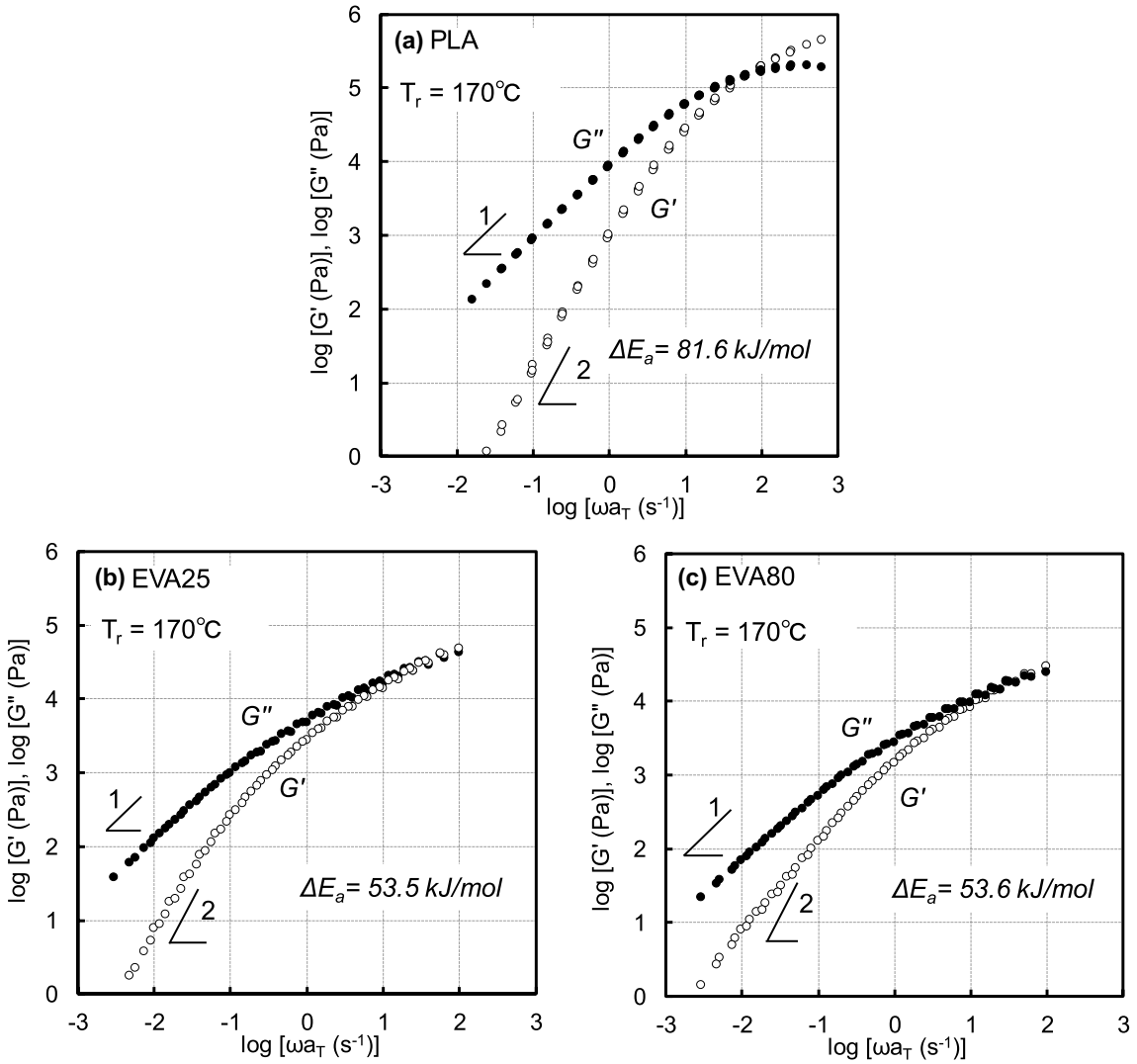

Fig. 1 Master curves of frequency dependence of shear storage modulus G' (open symbols) and loss modulus G'' (closed symbols) for **a** PLA, **b** EVA25, and **c** EVA80 at the reference temperature T_r of 170 °C. The apparent flow activation energy ΔE_a is denoted in the figure

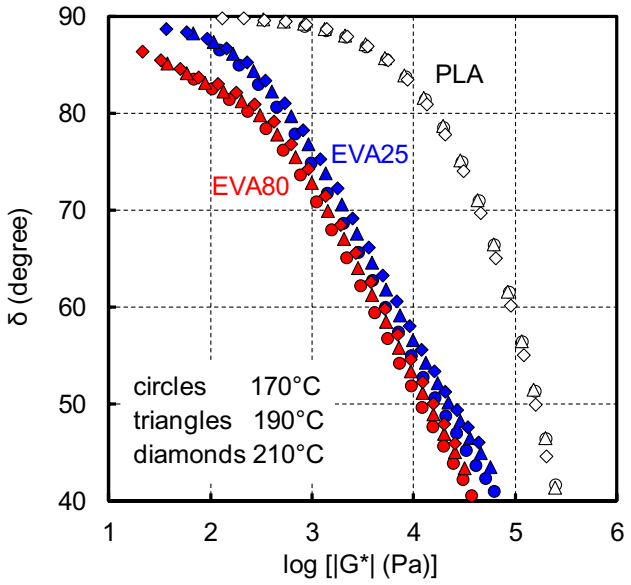

Fig. 2 Van Gurp-Palmen plots of pure samples: (circles) 170 °C, (triangles) 190 °C, and (diamonds) 210 °C

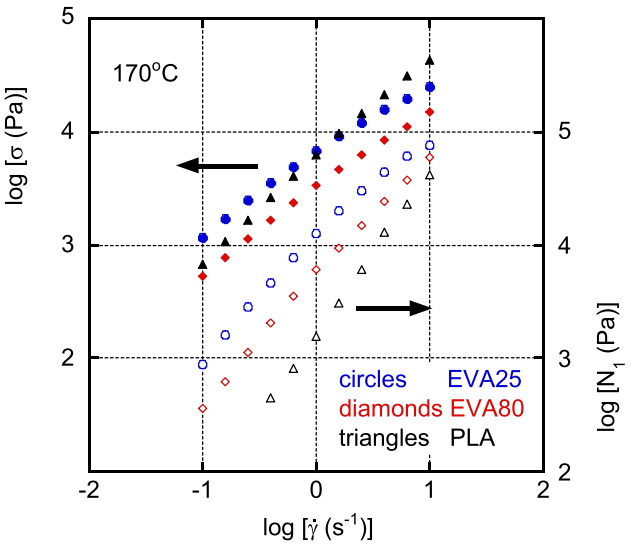

Fig. 3 Shear stress σ (closed symbols) and primary normal stress difference N_1 (open symbols) for PLA, EVA25, and EVA80 at 170 °C as a function of shear rate $\dot{\gamma}$

for the EVA samples, which is typical behavior for low-density polyethylene (LDPE) produced by radical polymerization under high pressure [34]. This is attributed to the high activation energy of the entanglement relaxation associated with long-chain branches [35, 36]. In contrast, all data collected at various temperatures were on the same curve for PLA.

Steady-state properties under shear flow, such as shear stress σ and primary normal stress difference N_1, for PLA, EVA25, and EVA80 at 170 °C are shown in Fig. 3. As can be seen in the figure, the shear stress of PLA is almost proportional to the shear rate except for in the high shear rate region, indicating that PLA shows Newtonian behavior over a wide range of shear rates. The slopes of shear stress for the EVA samples are lower than that of PLA, which is due to the broad distribution of relaxation time. In the high shear rate region, PLA shows the highest shear stress, whereas EVA80 shows the lowest shear stress in the experimental range of shear rate. In contrast, normal stress differences for EVA25 and EVA80 are higher than that of PLA. These findings were expected because EVA has a broad relaxation time distribution owing to its broad molecular weight distribution and long-chain branch structure.

Figure 4 shows the growth curves of uniaxial elongational viscosity η_E^+ at various Hencky strain rates $\dot{\varepsilon}$ for pure samples at 170 °C. The solid line in the figure represents three times the growth curve of shear viscosity in the linear region, i.e., 3 η^+, calculated from the oscillatory shear moduli shown in Fig. 1.

PLA exhibited no strain-hardening because of its linear molecular structure with narrow molecular weight distribution [3, 17, 19]. In contrast, EVA25 and EVA80 exhibited marked strain-hardening, similar to LDPE produced in an autoclave reactor [37, 38]. Since the extent of the strain-hardening is similar for EVA25 and EVA80, the difference in the branch structure between the samples must be insignificant.

Structure and Rheological Properties of PLA/EVA Blends

SEM images of the blend samples are shown in Fig. 5. The mean volume diameters of the dispersed droplets are 3.7 μm for PLA/EVA25 and 1.3 μm for PLA/EVA80. It is clear that the dispersed droplets of PLA/EVA80 (80/20) are fine compared with those of PLA/EVA25 (80/20), which is attributed to the difference in the interfacial tension. According to our previous study, the interfacial tensions between PLA and EVA were found to be 2.4 mN/m for PLA-EVA25 and 0.05 mN/m for PLA-EVA80 [4].

The master curves of the oscillatory shear moduli for the blends are shown in Fig. 6 at the reference temperature T_r of 170 °C. The solid lines in the figure denote the data for pure PLA. The G' values of PLA/EVA25 and PLA/EVA80 in the low frequency region were significantly higher than those of pure PLA, suggesting the existence of a long relaxation time mechanism attributed to the deformation of dispersed droplets [39–42]. According to the rheological emulsion model, the relaxation time of the droplet deformation τ_D and the corresponding second plateau modulus G_p are as follows:

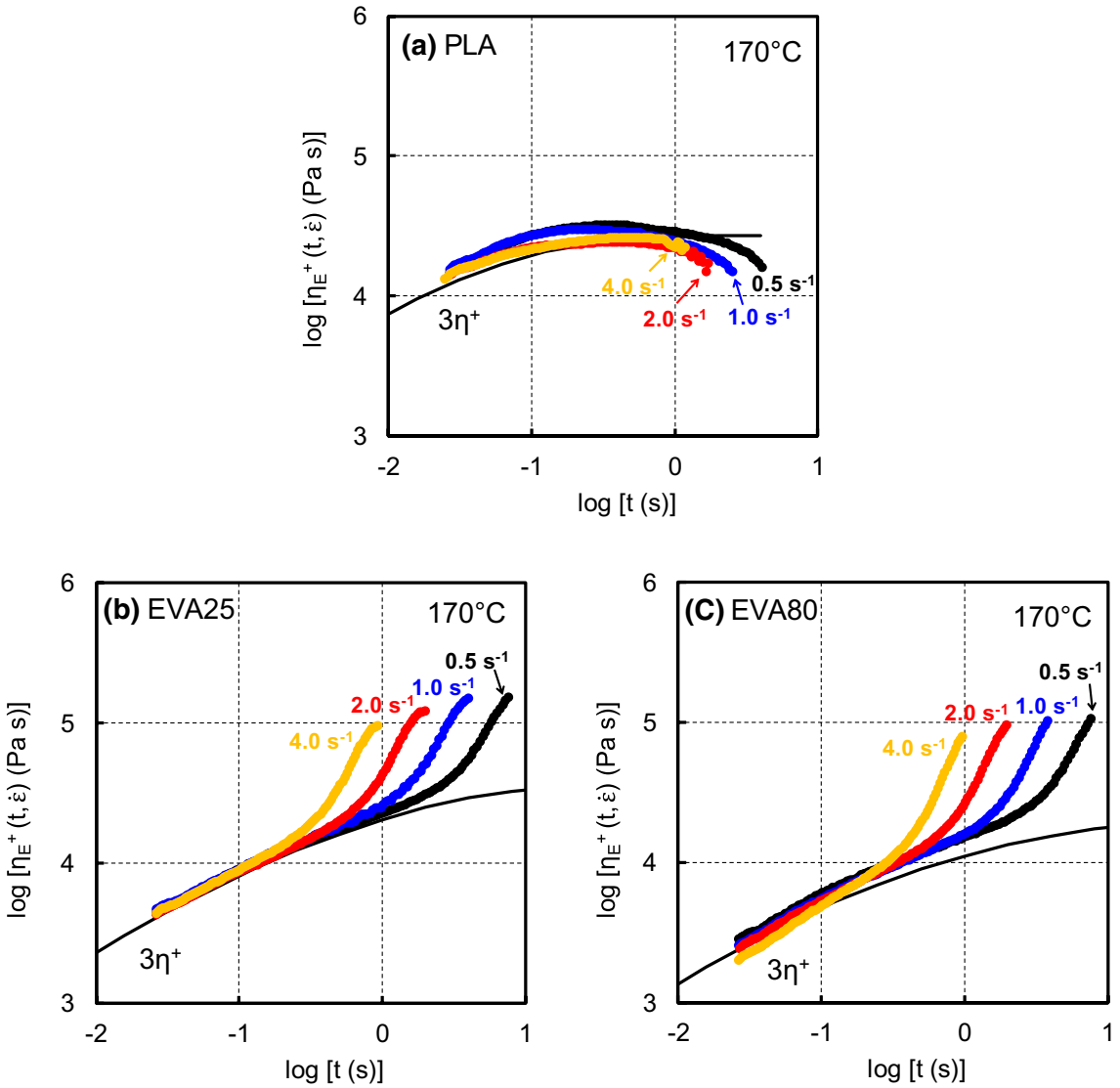

Fig. 4 Transient elongational viscosity over time at various Hencky strain rates at 170 °C: **a** PLA, **b** EVA25, and **c** EVA80

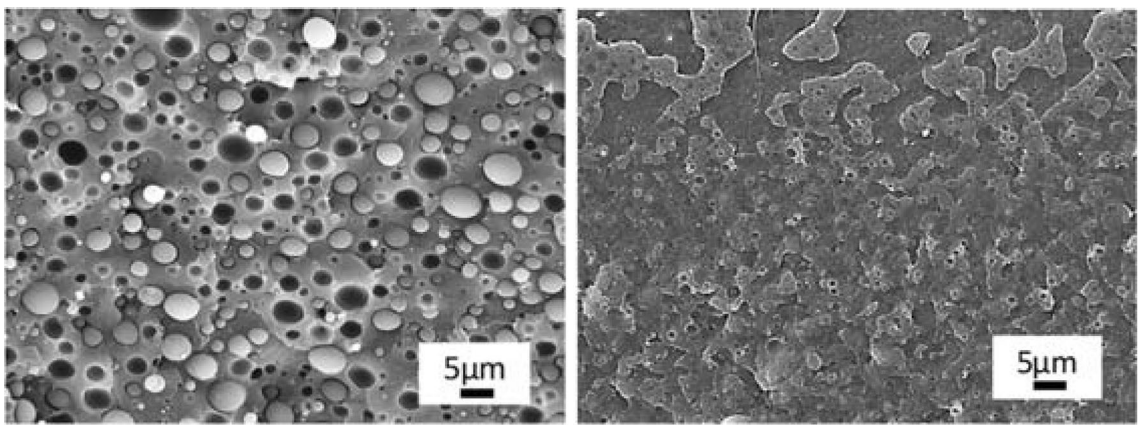

Fig. 5 SEM images of fractured surfaces of the PLA/EVA blends. (left)PLA/EVA25 and (right) PLA/EVA80

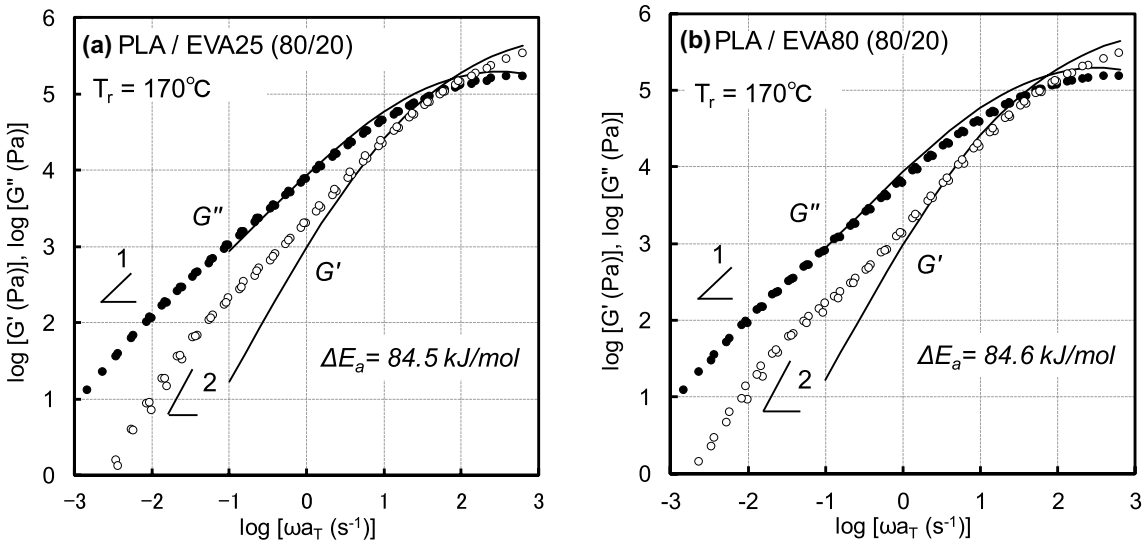

Fig. 6 Master curves for the frequency dependence of the shear storage modulus G' (open symbol) and loss modulus G'' (closed symbol) for **a** PLA/EVA25 (80/20) and **b** PLA/EVA80 (80/20). The solid lines denote the values for pure PLA

$$\tau_D = \frac{\eta_m R}{4\Gamma}\frac{(19K+16)(2K+3-2\phi(K-1))}{10(K+1)-2\phi(5K+2)} \tag{2}$$

$$G_p = \frac{20\Gamma\phi}{R}\frac{1}{(2K+3-2\phi(K-1))^2} \tag{3}$$

$$K = \frac{\eta_d}{\eta_m} \tag{4}$$

where η_d and η_m are the viscosities of the dispersion and matrix, respectively, Γ is the interfacial tension, R is the radius of the dispersed droplets, and ϕ is the volume fraction of the dispersion.

The secondary plateau modulus of PLA/EVA25 was slightly higher than that of PLA/EVA80, which is attributed to the difference in Γ/R; i.e., the high interfacial tension between PLA and EVA25 is responsible for the high value of the secondary plateau.

Figure 7 shows the steady-state properties under shear flow, such as shear stress and primary normal stress difference, for PLA/EVA25 and PLA/EVA80 at 170 °C with the data for pure PLA. The shear stress was barely affected by the addition of EVA. Moreover, the primary normal stress differences of the blends were higher than those of the pure PLA at low shear rate. Since the shear viscosity of PLA was not significantly different to those of the EVA samples in the shear rate region, the contribution of interfacial tension cannot be ignored as predicted by the Doi–Ohta theory [43]. In the high shear rate region, however, the difference became minimal. Consequently,

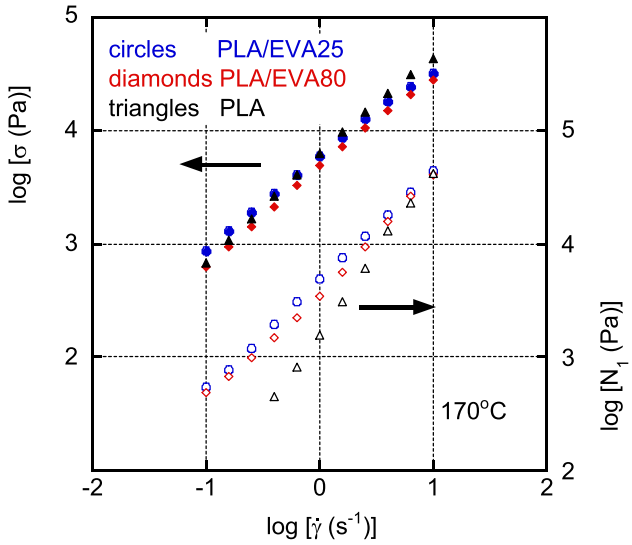

Fig. 7 Shear stress σ (closed symbols) and primary normal stress difference N_1 (open symbols) for PLA, PLA/EVA25 (80/20), and PLA/EVA80 (80/20) at 170 °C as a function of shear rate $\dot{\gamma}$

the slope in the figure became gentle for the blends and almost 1 over the wide range of shear rates.

The transient uniaxial elongational viscosity η_E^+ for the blends is shown in Fig. 8. Strain-hardening behavior, which was not detected for pure PLA, was clearly detected on the addition of EVA with an intense fashion of PLA/EVA25. The mechanism for the strain-hardening was explained in our previous papers [22, 23]. According to those reports, the dispersion with slightly lower viscosity is deformed affinely with the deformation of the matrix at the early stage

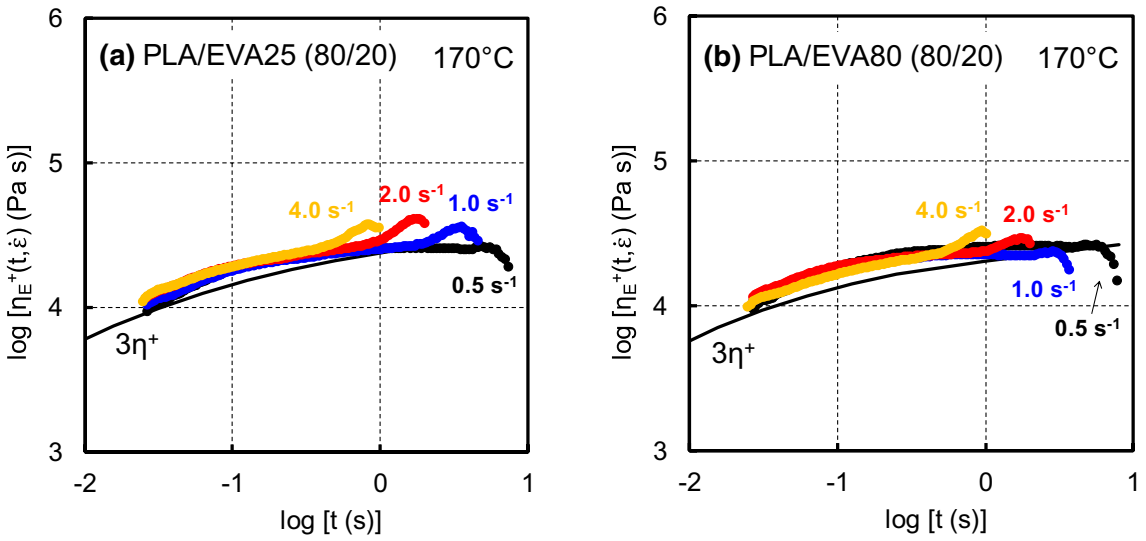

Fig. 8 Transient elongational viscosity over time at various Hencky strain rates at 170 °C: **a** PLA/EVA25 (80/20) and **b** PLA/EVA80 (80/20)

of elongational flow. Eventually, the droplets showed almost no deformation owing to their strain-hardening and behaved like rigid fibers. The matrix between the rigid fibers has to be greatly deformed under elongational flow, leading to excess stress generation, i.e., strain-hardening. Compared with EVA80, EVA25 has higher elongational viscosities over the entire time/strain region. As a result, the droplets of EVA25 become "rigid" within a shorter time/strain region than those of EVA80.

Film Processability and Mechanical Properties

Figure 9 shows the appearance of the tubular-blown films. Because pure PLA shows no strain-hardening in the transient elongational viscosity, the film bubble was unstable. Furthermore, it was not possible to prepare a pure PLA film with 10 µm thickness. In contrast, the bubble was stable for PLA/EVA25 (80/20) and a 10 µm thick film was successfully prepared.

The mechanical properties of the tubular-blown films with 30 µm thickness were also evaluated, as summarized in Table 1 with standard deviation. It has been well known that the improvement of mechanical toughness is greatly required for PLA films [1–4, 44]. As discussed in our previous paper [4], in which we revealed the effect of the vinyl acetate content in EVA on the film properties, the addition of EVA provides PLA with flexibility and ductile nature. As a result, the blend film showed low modulus and high elongation at break compared with pure PLA. Furthermore, the tear strength was improved. It should be mentioned that mechanical anisotropy was clear for the blend, suggesting that the chain orientation in MD was enhanced. This is reasonable because the blend shows

Fig. 9 Processability of tubular-blown films with 30 µm thickness

strain-hardening in the elongational viscosity. As revealed by several researchers, strain-hardening is responsible for the formation of shish-kebab structure in the tubular-blown film, leading to a high degree of molecular orientation [45–49].

Table 1 Mechanical properties of the films

Sample	Direction	Tensile modulus (MPa)	Elongation at break (%)	Tear strength (kN/m)
PLA	MD	1500	4.0 ± 0.5	5.2 ± 0.3
	TD	1450	4.0 ± 0.2	5.1 ± 0.5
PLA/EVA25 (80/20)	MD	1100	38.0 ± 4.6	12.4 ± 2.4
	TD	720	82.4 ± 19.7	17.7 ± 2.5

MD machine direction, *TD* transverse direction

Conclusions

The addition of ethylene–vinyl acetate copolymer (EVA) enhances the melt elasticity of poly(lactic acid) (PLA). The droplet size of EVA decreases with increasing the vinyl acetate content due to a low interfacial tension. Under shear flow, the primary normal stress difference is greatly enhanced, particularly in the low shear rate region, which is attributed to the increase in the interfacial area as revealed by the Doi–Ohta theory. Under elongational flow, strain-hardening behavior—one of the most important elastic behaviors required for various processing operations—is detected following EVA addition irrespective of the vinyl acetate content, even though EVA is in the dispersed phase. Because the blend shows strain-hardening in the elongational viscosity, the film processability in tubular-blown film extrusion is greatly improved, showing a stable bubble. Moreover, the mechanical toughness such as elongation at break and tear strength is enhanced significantly. Since a thin film can be prepared as a result of EVA addition, this technique will almost certainly be employed in industry.

References

1. Auras R, Lim LT, Selke SEM, Tsuji H (2010) Poly(lactic acid): synthesis, structures, properties, processing, and applications. Wiley, Hoboken
2. Jimenez A, Peltzer M, Ruseckaite R (2014) Poly(lactic acid) science and technology: processing, properties, additives, and applications. RSC Publishing, Oxfordshire
3. Yamaguchi M (2017) Manufacturing of high performance biomass-based polyesters by rheological approach. In: Thakur VK, Thakur MK, Kessler MR (eds) Handbook of composites from renewable materials. Wiley, Hoboken
4. Kugimoto D, Kouda S, Yamaguchi M (2019) Polym Test 80:106021
5. Satoh N, Tomiyama H, Kajiwara T (2001) Polym Eng Sci 41:1564
6. Yamaguchi M, Suzuki K (2001) J Polym Sci B 39:2159
7. Yamaguchi M, Suzuki K, Maeda S (2002) J Appl Polym Sci 86:73
8. Yamaguchi M, Suzuki K (2002) J Appl Polym Sci 86:79
9. Yamaguchi M, Todd DB, Gogos CG (2003) Adv Polym Technol 22:179
10. Kouda S (2008) Polym Eng Sci 48:1094
11. Yamaguchi M (2014) Material strength in molten state for foam. In: Lee ST, Park CB (eds) Foam extrusion: principles and practice, 2nd edn. Wiley, New York
12. Wang L, Jing X, Cheng H, Hu X, Yang L, Huang Y (2012) Ind Eng Chem Res 51:10731
13. Gu L, Xu Y, Fahnhorst GW, Macosko CW (2017) J Rheol 61:785
14. Yamaguchi M, Wakabayashi T (2006) Adv Polym Technol 25:236
15. Nofar M, Zhu W, Park CB, Randall J (2011) Ind Eng Chem Res 50:13789
16. Li Y, Mi J, Fu H, Zhou H, Wang X (2019) ACS Omega 4:12512
17. Amran BMAM, Okamoto K, Yamaguchi M, Koshirai A, Kasai T (2009) J Polym Sci B 47:2008
18. Yokohara T, Nobukawa S, Yamaguchi M (2011) J Rheol 55:1205
19. Yamaguchi M, Fukuda K, Yokohara T, Amran BMAM, Nobukawa S (2012) Macromol Mater Eng 297:654
20. Yamaguchi M, Yokohara T, Ali MABM (2013) J Soc Rheol Jpn 41:129
21. Kang GB, Kim MH, Son Y, Park OO (2009) J Appl Polym Sci 111:3121
22. Fujii Y, Nishikawa R, Phulkerd P, Yamaguchi M (2019) J Rheol 63:11
23. Otsuki Y, Fujii Y, Sasaki H, Phulkerd P, Yamaguchi M (2020) Polym J 52:529
24. Batchelor GK (1971) J Fluid Mech 46:813
25. Mewis J, Metzner AB (1974) J Fluid Mech 62:593
26. Laun HM (1984) Colloid Polym Sci 262:257
27. Yamaguchi M, Fuji Y, Phulkerd P (2020) J Soc Rheol Jpn 48:109
28. Peón J, Vega JF, Aroca M, Salazar JM (2001) Polymer 42:8093
29. Gupta RK, Zujo VP, Bhattacharya SN (2005) J Non-Newtonian Fluid Mech 128:116
30. Gajria AM, Dave V, Gross RA, McCarthy SP (1996) Polymer 37:437
31. Small PA (1953) J Appl Chem 3:71
32. Huang T, Miura M, Nobukawa S, Yamaguchi M (2014) J Polym Environ 22:183
33. Gurp MV, Palmen J (1998) Rheol Bull 67:55
34. Wagner MH, Kheirandish S, Yamaguchi M (2004) Rheol Acta 44:198
35. Raju VR, Rachapudy H, Graessley WW (1979) J Polym Sci B 17:1223
36. Siriprumpoonthum M, Nobukawa S, Satoh Y, Sasaki H, Yamaguchi M (2014) J Rheol 58:449
37. Yamaguchi M, Takahashi M (2001) Polymer 42:8663
38. Wagner MH, Yamaguchi M, Takahashi M (2003) J Rheol 47:779
39. Graebling D, Muller R, Palierne JF (1993) Macromolecules 26:320
40. Yamaguchi M, Miyata H (1999) Macromolecules 32:5911
41. Yokohara T, Yamaguchi M (2008) Eur Polym J 44:677
42. Yokohara T, Okamoto K, Yamaguchi M (2010) J Appl Polym Sci 117:2226
43. Doi M, Ohta T (1991) J Chem Phys 95:1242
44. Huang T, Miura M, Nobukawa S, Yamaguchi M (2015) Biomacromol 16:1660

45. Wang J, Bai J, Zhang Y, Fang H, Wang Z (2016) Sci Rep 6:26560
46. Wingstrand SL, Drongelen M, Mortensen K, Graham RS, Huang Q, Hassager O (2017) Macromolecules 50:1134
47. Zhang Q, Li L, Su F, Ji Y, Ali S, Zhao H, Meng L, Li L (2018) Macromolecules 51:4350
48. Jalali A, Huneault MA, Nofar M, Lee PC, Park CB (2019) Eur Polym J 119:410
49. Nishikawa R, Yamaguchi M (2019) J Appl Polym Sci 136:48010